Citation: The Journal of the Acoustical Society of America **149**, 87 (2021); doi: 10.1121/10.0002943

Nonlinear crosstalk in broadband multi-channel echosounders

Babak Khodabandeloo, Egil Ona, Gavin J. Macaulay, Rolf Korneliussen

Ecosystem Acoustics Group, Institute of Marine Research, Bergen, Norway

Abstract

Distortion of acoustic wave caused by nonlinear propagation transfers acoustic energy into higher harmonics of the transmitted signal. When operating several broadband echosounders with non-overlapping frequency bands to cover a wide frequency range, higher harmonics generated by one band may interfere with the fundamental band of others. This interference (i.e., crosstalk), can adversely affect the measured backscattered amplitude frequency response and in some circumstances appears as spurious targets above and/or below the main target in pulse-compressed echograms. The nonlinear propagation of frequency-modulated acoustic waves in a directional beam was modeled and used to assess methods to reduce the deleterious effects of harmonic components in the signal and was also compared to field experiments using the seabed echo and a metallic target sphere, with good agreement. Two methods are shown to materially reduce crosstalk: 1) reduction in transmit power, which reduces crosstalk amplitude by a larger amount than the associated reduction in transmit power, and 2) selection of a proper Fourier window length in the processing stage. The effect of crosstalk was small (<0.4 dB or 10%) for area backscattering measurements, but could be several dB for target strength measurements at different frequencies depending on the transmit signals and processing parameters.

I. INTRODUCTION

Echosounders are used to transmit acoustic energy within pre-determined and specific frequency bands. For acoustic pulses of finite duration, some of the energy is transmitted out of the band due to the non-sinusoidal shape of the pulse envelope (Proakis and Manolakis, 1996) and the physical inertia of the acoustic transducer elements. More significantly, distortion of the acoustic waveform generates energy leakage at harmonics of the fundamental frequencies. Wave distortion can be due to

instrumentation nonlinearity (Liu et al., 2011) and signal clipping (Kuo et al., 2004) caused by the transmission or measurement process. Furthermore, wave distortion can be physics-based, being accumulated through nonlinear acoustic propagation from the dependence of the acoustic wave propagation speed on pressure (Hamilton and Blackstock, 1998). When the pressure amplitude is sufficiently high, this latter effect distorts the pulse waveform as it propagates through the medium. As a consequence of the Fourier series representation of non-sinusoidal signals, waveform distortions require some of the acoustic energy to exist at harmonic frequencies of the intended frequency or band. These harmonics can be beneficial, such as for medical imaging (Duck, 2002) and nondestructive ultrasonic material evaluation (Matlack et al., 2015) but the presence of harmonics, regardless of their origin, are generally unwanted in quantitative uses of echosounders for fisheries acoustics.

Echosounders have been used to observe biological targets in aquatic environments since the 1930's (Sund, 1935) and are now commonly used to provide biomass estimates of aquatic organisms, especially exploited fish populations and hence are important tools for the assessment and scientific advice on the management of marine resources (Simmonds and MacLennan, 2005, Chapter 3; Trenkel et al., 2011). Integrated backscattered energy is used to derive biomass, given that the scattering properties of representative individuals within the stock are known.

Most scientific echosounders transmit a narrowband pulsed acoustic signal. The use of several simultaneously operated echosounder-channels, at well-separated narrowband acoustic frequencies is common (Holliday, 1989; Korneliussen and Ona, 2002). The variation with frequency of the backscattered intensity between different types of organisms can be used to distinguish between target categories, or even target species. This method is termed the multi-frequency approach (Korneliussen and Ona, 2002).

A natural extension of the multi-frequency approach is to increase the number of narrowband frequencies (Greenlaw, 1979) or to use broadband instead of narrowband transmit signals (Stanton et al., 2003; Chu, 2011; Korneliussen et al., 2016). Broadband pulses can have additional benefits such as an improved range resolution (being proportional to the inverse of the transmitted signal's bandwidth rather than the pulse duration) and an improved signal-to-noise ratio (SNR), both achieved using signal processing techniques such as matched filtering (Price, 1956; Chu and Stanton, 1998; Stanton et al., 2003). The use of broadband backscatter can also improve the identification of organisms through a

near-continuous frequency resolution (Stanton et al., 2010; Andersen et al., 2013; Korneliussen et al., 2016; Bassett et al., 2018). The increased range resolution provided by broadband pulses enables single targets to be measured in higher volume densities than with narrowband pulses (Chu and Stanton, 1998) for a given SNR.

The nonlinear loss in echosounders can be significant, causing measured backscatter to be dependent on transmit power and target range. For example, Tichy et al. (2003) showed that at 200 kHz, increasing the transmit power from 56 to 280 W resulted in a ~1 and ~2 dB drop in backscattered signal at target ranges of 5 and 10 m, respectively. Korneliussen et al. (2008) have recommended power settings for commonly-used transducers to avoid significant nonlinear effects. When combined with the use of calibration spheres beyond a range where most of the nonlinear generation of sound occurs (approximately 10-15 m), the calibration compensates for the non-linear loss at the fundamental frequency. This approach could be considered an oversimplification if the purpose was solely to avoid significant nonlinear generation of sound but are sufficient in multi-frequency systems when combined with carefully chosen operating frequencies (Korneliussen et al., 2008). For broadband multi-channel echosounders, however, this method is not sufficient as the higher harmonic frequencies at one broadband channel cannot be avoided at the higher frequency broadband channels. Thus, a different approach than the one used by Korneliussen et al. (2008) is needed.

An undesirable effect of energy leakage into higher harmonics is crosstalk or cross-channel interference which occurs when operating several transducers simultaneously. That is, a channel can receive energy that was generated by another channel, and if unaccounted for can cause bias in quantitative measures of backscatter amplitude. The frequencies typically used in multi-frequency fisheries echosounder systems (18, 38, 70, 120, 200, and 333 kHz) have been chosen to reduce this bias by using frequencies which are not harmonics of the lower frequencies. However, with a broadband pulse, the emitted higher-order harmonics cover a wide frequency range which is more difficult to avoid. For example, a 50 — 90 kHz signal also generates energy at frequencies that are twice (100 — 180 kHz) and three times (150 — 270 kHz) the original, which can be detected by echosounder channels which are listening at, for example, 95 — 160 kHz and 160 —260 kHz (these are commonly-used broadband frequency ranges). The cross-channel interference, if not the magnitude, was recognized soon after starting the use of quantitative multi-channel broadband echosounders (Andersen et al., 2013) and resolved by transmitting on the echosounder channels sequentially, rather than simultaneously. The inevitable

consequence of this was a potentially large reduction in the per channel ping rate (Blanluet et al., 2019). More recent studies have quantified the level of bias as potentially significant (Demer et al., 2017) but in some situations the practical effect appears to be undetectable (Jech et al., 2017).

The potential bias due to crosstalk can result in an incorrect relative frequency response which in turn can lead to wrong target identification when using frequency response-based backscatter classification (Korneliussen and Ona, 2002; Horne, 2000; Korneliussen et al., 2016; Bassett et al., 2018). When using multiple broadband transducers, the other consequence of crosstalk is the appearance of target artifacts in pulse-compressed echograms, close in range to the true target range. This will adversely affect existing single echo detectors (SED) which rely on clean single target echoes with no spurious side-targets within the same band (Ona, 1999; Handegard, 2007). Furthermore, nonlinear losses can also 'flatten' the transducer beampatterns since the nonlinear effect is stronger when the pressure amplitude is higher, such as on the acoustic axis compared to off axis. Hence, the higher the transmit power, the more flattened the transducer beampattern compared to that predicted by linear acoustic theory. If not accounted for, the measured backscatter amplitude from organisms within the beam may be incorrect (Pedersen, 2006).

In the applications where the disadvantages of cross-talk outweigh the benefits of simultaneous pinging at full power, the non-linearly generated sound must be made negligible in some way. A common echosounder configuration has six channels centered on 18, 38, 70, 120, 200, and 333 kHz and several methods are possible to achieve this:

- Operate the channels sequentially i.e. only operate one channel at a time. However, this creates a low ping rate for individual channels (e.g., 1/6 of full ping rate) that is typically inadequate for sampling resolution reasons.
- Group the various channels in a manner that minimizes harmonic crosstalk and then operate these channel groups sequentially.
- Restrict the bandwidth of each channel so that crosstalk is avoided. This significantly reduces the frequency band coverage.
- Reduce the interference effects in the processing stage.
- Change the characteristics of the transmit pulse to reduce the generation of harmonic energy.

In this paper, we focus on the last item above by simulating the harmonic generation of broadband echosounder signals due to nonlinear acoustic wave propagation and comparing these modeling results to field measurements. Numerical modeling enables us to isolate the physics-based harmonic generation from those potentially caused by the instrumentation. From these investigations, we show the effects of different transmit power settings on the level of generated crosstalk. In addition, the possibilities for reducing crosstalk interference using different processing parameters is investigated. The consequences of each method are presented, with the aim of providing assistance and insight into selecting an appropriate strategy that meets data acquisition requirements.

II. METHODS

A. Nonlinear propagation model

The Khokhlov-Zabolotskaya-Kuznetsov (KZK) equation is a nonlinear parabolic wave equation modeling the propagation of finite amplitude acoustic waves in a sound beam (Novikov et al., 1987). At high frequencies (*ka* >> 1, where *a* is the source radius and *k* is the wave number), the KZK equation has been shown to be an accurate model for the sound field generated by a directional source beyond a few source radii and in the region up to 20° off the beam axis (Averkiou and Hamilton, 1997). This is appropriate for the 5-10° beamwidth transducers typically used for acoustic biomass estimation. The model considers the combined effects of diffraction, nonlinearity, thermos-viscous absorption and an arbitrary number of independent relaxation phenomena (Cleveland et al., 1996; Lee and Hamilton, 1995). In a cylindrical coordinate-system the equation is written as:

$$\frac{\partial p}{\partial z} = \int_{-\infty}^{t'} \frac{c_0}{2}\left(\frac{\partial^2 p}{\partial r^2} + \frac{1}{r}\frac{\partial p}{\partial r}\right) dt'' + \frac{\beta}{2\rho_0 c_0^3}\frac{\partial p^2}{\partial t'} + \frac{\delta}{2c_0^3}\frac{\partial^2 p}{\partial t'^2} + \sum_{\nu}\frac{c_\nu'}{c_0^2}\int_{-\infty}^{t'}\frac{\partial^2 p}{\partial t''^2} e^{-(t'-t'')/t_\nu} dt'', \quad (1)$$

where c_0 (m/s) and ρ_0 (kg/m^3) are the speed of sound and density of water, respectively. $\beta = 1 + B/2A$ is the coefficient of nonlinearity, p (Pa) is pressure, and δ (m^2/s) is the diffusivity of sound in a thermo-viscous fluid (Hamilton and Morfey, 1998); $r, \theta,$ and z are cylindrical coordinates where z is the main direction of propagation; $t' = t - z/c_0$ is the retarded time, c_ν' is a small signal sound speed increment,

and $t_\nu = 1/2\pi f_\nu$ is the relaxation time where f_ν is the corresponding relaxation frequency for each relaxation phenomena.

Eq. (1) is solved by a finite-difference time domain algorithm as implemented by the KZK Texas code (Lee, 1993; Lee and Hamilton 1995). This algorithm transforms Eq. (1) into a dimensionless form via the following transformations:

$$P = (1+\sigma)(p/p_0),\ \sigma = z/z_0,\ \rho = (r/a)/(1+\sigma),\ \tau = \omega_0 t' - (r/a)^2/(1+\sigma), \tag{2}$$

where p_0 is the uniform pressure on the transducer surface, and $z_0 = \omega_0 a^2/2c_0$ is the Rayleigh-distance. The effects of diffraction, nonlinearity, absorption and relaxation are included term by term separately at each marching step from σ to $\Delta\sigma$, by the following equations, respectively:

$$\frac{\partial P}{\partial \sigma} = \frac{1}{4(1+\sigma)^2}\int_{-\infty}^{\tau}\frac{c_0}{2}\left(\frac{\partial^2 P}{\partial \rho^2} + \frac{1}{\rho}\frac{\partial P}{\partial \rho}\right)d\tau', \tag{3}$$

$$\frac{\partial P}{\partial \sigma} = \frac{NP}{(1+\sigma)}\frac{\partial P}{\partial \tau'}, \tag{4}$$

$$\frac{\partial P}{\partial \sigma} = A\frac{\partial^2 P}{\partial \tau^2}, \tag{5}$$

$$\left(1 + \theta_\nu \frac{\partial}{\partial \tau}\right)\frac{\partial P}{\partial \sigma} = C_\nu \frac{\partial^2 P}{\partial \tau^2}. \tag{6}$$

In the above equations, $N = z_0/\bar{z}$ and $A = \alpha_0 z_0$ are the non-dimensional nonlinearity and viscous absorption, respectively. Here $\bar{z} = \rho_0 c_0^3/\beta\omega_0 p_0$ is the plane-wave shock formation distance and α_0 (Np/m) is the thermo-viscous attenuation coefficient. The relaxation parameters $C_\nu = \mathrm{c}_\nu' t_\nu z_0 \omega_0^2/c_0^2$ and $\theta_\nu = \omega_0 t_\nu$ are the parameters for the included relaxation processes (Lee and Hamilton, 1995).

The absorption of acoustic waves in seawater is considered mainly as the sum of the thermo-viscous absorption from pure water and two relaxation phenomena due to boric acid and magnesium sulfate. The thermo-viscous attenuation coefficient and the relaxation frequencies of boric acid and magnesium sulfate can be estimated (Francois and Garrison, 1982). The small signal sound speed increment, c_ν', for the boric acid and magnesium sulfate relaxation phenomenon were obtained from the literature (Pierce, 1989, Chapter 10, Rossing, 2007, Chapter 3)

1. Pressure on the transducer surface

The pressure on the transducer surface, p_0, is required by the KZK Texas code and subsequent analyses and an estimate of p_0 from a given input power to the transducer is also needed. To obtain this, radiated power, W, by a source is obtained by (Lawrence et al., 2000 Chapter 7; Pierce, 1989 Chapter 5):

$$W = W_{in}\eta_{rad}\eta_{el-ac} = \frac{1}{2}U_a^2 R_r. \quad (7)$$

where U_a is the surface velocity of transducer, W_{in} is the input power, η_{rad} is the acoustic radiation efficiency, η_{el-ac} is the electroacoustic efficiency of the transducer, and R_r is the real part of acoustic radiation impedance which is the ratio of force amplitude F_0 to the normal velocity amplitude U_a. The radiation impedance of a baffled piston is estimated by (Lawrence et al., 2000 Chapter 7; Pierce, 1989 Chapter 5):

$$Z_r = \frac{F_0}{U_a} = R_r + jXr = \rho c S_0 \left[\left(1 - \frac{2J_1(2ka)}{2ka}\right) + j\frac{2H_1(2ka)}{2ka}\right]. \quad (8)$$

where J_1 and H_1 are Bessel and Struve functions of the first order, respectively. The area of the transducer face is given by S_0. For a given transducer, R_r is given by Eq. (8) and U_a is estimated from Eq. (7). Subsequent to calculating F_0 from Eq. (8), pressure on the transducer face can be estimated from:

$$p_0 = \frac{|F_0|}{a^2\pi}. \quad (9)$$

For small wavelengths compared to the transducer radius a good approximation to the pressure on the transducer surface can be obtained from (Lawrence et al., 2000):

$$W = a^2\pi I = a^2\pi\frac{p_0^2}{2\rho_0 c_0} \quad (10)$$

B. Simulations

The nonlinear acoustic propagation was simulated for four broadband transducers (the ES38-7, ES70-7C, ES120-7C, and ES200-7C, with nominal operating frequencies of 38, 70, 120, and 200 kHz, all produced by Kongsberg Maritime, Norway) with the assumption that they operated as a uniform piston source of radius a. However, in order to reduce the amplitude of beam side lobes, the power to specific elements in these transducers are weighted (Stanton et al., 2010). The effective radius of a uniform piston was estimated by curve fitting the main lobe of the theoretical directivity for a plane circular piston (Lawrence et al., 2000, Chapter 7) to the measured directivity based on minimization of least squares (Table *1*).

Table 1. Frequency ranges and surface area of four transducers. f_{nom} is a nominal frequency for the transducer and the effective circular radium was obtained from Korneliussen et al. (2008).

Transducer model	$f_{nom}\ (kHz)$	Frequency range (kHz)	Effective circular radius (mm)	Directivity estimated radius (mm)
ES38-7	38	34-45	178	160
ES70-7C	70	45-90	98	85
ES120-7C	120	90-170	56	51
ES200-7C	200	160-260	37	28

C. Experiments

Two field experiments were carried out in order to verify the model and the effectiveness of crosstalk reduction for simultaneous operation of broadband echosounders. The first compared the backscattering from a flat seafloor at different power settings. The seafloor is a strong reflector, and therefore suits observation of higher harmonics (which are weaker compared to the fundamental band) especially when transmit power is reduced. The second experiment compared the backscattering from a small metallic calibration sphere. We can therefore evaluate the seafloor measurement as a good measurement of the relative effect, while the sphere measurement one may be regarded as absolute with respect to accuracy.

1. Experiment 1: (Higher harmonics observation by seafloor measurements)

A Kongsberg Maritime EK80 echosounder system, operating with broadband pulses of 34-45, 45-90, 90-160, and 160-260 kHz, was used to evaluate and measure the crosstalk occurring from seafloor echoes. The echosounders were mounted on the hull of the Institute of Marine Research (IMR) research vessel RV "G.O. Sars" and anchored in Sandviksflaket, Bergen, Norway, on 16 September 2019. The range to the seafloor was about 40 m and backscatter from the seafloor echo was relatively insensitive to frequency. The level of crosstalk was measured by operating one echosounder channel with various transmit power levels while listening with the other channels (Table 2). For volume backscattering calculations, the range was selected from 2 meters above the seafloor to 6 meters below (i.e. 8 m window) and 200 pings were used for averaging. Increasing the depth range for calculation of volume backscattering strength (S_v) will change the absolute levels but not the shape of the curve. The mean value of volume backscattering with 95% confidence interval were calculated using the standard error of the mean (sem) function in the SciPy statistical module (Jones et al., 2001), a Python library.

Table 2. Echosounder channel configurations used to measure crosstalk levels. The passive channels do not emit sound but do record received signals.

	34-45 kHz		45-90 kHz		90-160 kHz		160-260 kHz	
Meas. id	Power (W)	Mode	Power (W)	Mode	Power (W)	Mode	Power (W)	Mode
1	2000	Active	750	Passive	250	Passive	105	Passive
2	1000	Active	750	Passive	250	Passive	105	Passive
3	600	Active	750	Passive	250	Passive	105	Passive
4	200	Active	750	Passive	250	Passive	105	Passive
5	2000	Passive	750	Active	250	Passive	105	Passive
6	2000	Passive	600	Active	250	Passive	105	Passive
7	2000	Passive	300	Active	250	Passive	105	Passive
8	2000	Passive	75	Active	250	Passive	105	Passive
9	2000	Passive	750	Passive	250	Active	105	Passive
10	2000	Passive	750	Passive	250	Passive	105	Active

a. Relation between volume backscattering and normalized incident pressure

The volume backscattering coefficient, s_v (m^{-1}) is derived from the emitted and received acoustic energy from the insonified target for which the effects of absorption and geometrical spreading have been compensated. The nonlinear generation of sound is considerable from echosounder to the target (here seafloor), while the propagation from target to echosounder can be considered linear because the backscattered pressure is much smaller than the incident pressure and therefore the nonlinear generation of sound is negligible. In this section the relationship between S_v ($= 10\log_{10}(s_v)$, dB re 1 m^{-1}) and the incident pressure at the target is presented. This is achieved by simulating the pressure, including non-linear effects, incident upon the target.

The volume backscattering coefficient is defined as (Medwin and Clay 1998, chapter 9):

$$s_v(f) = 2\frac{R^2 10^{\frac{\alpha(f)R}{5}} \sum_{i=1}^{N} \int_{t_1}^{t_2} \left|p_{rec,i}(t)\right|^2 dt}{\psi_D c\,(t_2 - t_1) R_0^2 \int_0^{t_d} |p_{R0}(t)|^2 dt}, \tag{11}$$

where $p_{rec,i}$ is the received pressure by the transceiver due to the backscattering from target "i" within the volume, R is the distance from target to the transceiver, p_{R0} is the pressure at R_0 from the source which is normally 1 m, N is the number of targets within the volume, ψ_D is the integrated beam pattern, t_1 and t_2 specify the time gate in the receiver which in fact determine the gated volume, t_d is the incident ping duration, and α (dB/m) is the acoustic absorption. Assuming a uniform seafloor within the insonified beam at each ping, the above equation can be rewritten as:

$$s_v(f) = \frac{2R^2 10^{\frac{\alpha(f)R}{5}}}{t_d \psi_D c R_0^2} \frac{p_{rec}^2(t)}{p_{R0}^2(t)}, \tag{12}$$

where p_{rec} is the received pressure by the transducer on the acoustic axis ($D_t = 1$). It is expressed in terms of the incident pressure to the target as (Medwin and Clay, 1998, Chapter 4):

$$p_{rec}^2 = \frac{{D_t}^2 p_{inc}^2 \sigma_{bs}}{R^2} 10^{\frac{-\alpha\,(f)\,R}{10}} \tag{13}$$

where p_{inc} is the incident pressure to the target, that is the pressure just before arriving to the target, σ_{bs} is the backscattering cross section, and D_t is the transducer directional pressure response which is

equal to one on the acoustic axis. Replacing the received pressure in Eq. (12) by the one in Eq. (13) gives

$$s_v(f) = \frac{2R^2 10^{\frac{\alpha(f)R}{5}}}{t_d \psi_D c R_0^2} \frac{p_{inc}^2(t)}{p_{R0}^2(t)} \frac{{D_t}^2 \sigma_{bs}}{R^2} 10^{\frac{-\alpha\,(f)\,R}{10}}, \tag{14}$$

and sorting the above equation by grouping the absorption terms and taking 10 times the logarithm of both sides produces:

$$S_v(f) - 10\log_{10}\left(\frac{2{D_t}^2}{t_d \psi_D c R_0^2}\right) - 10\log_{10}(\sigma_{bs}) - \alpha\,(f)\,R = 10\log_{10}\left(\frac{p_{inc}^2(t)}{p_{R0}^2(t)}\right) \tag{15}$$

Since $\psi_D \sim D_t^2$, the second term on the left-hand side is frequency independent and therefore does not change the shape of the estimated volume backscattering coefficient curves. On the other hand, the third and fourth terms are frequency dependent and their effect should be removed from the measured S_v to have a correct comparison between normalized simulated incident pressure (given in section II.B) and the normalized measured volume backscattering.

2. Experiment 2: (TS measurement by synchronized operation of the broadband echosounders)

The backscatter from a 38.1 mm diameter tungsten carbide sphere (with 6% cobalt binder) was measured using four broadband echosounders (nominally 38, 70, 120, and 200 kHz) mounted on the hull of RV “G.O. Sars”. The vessel was anchored in 40 m water depth in Grøssvikvågen, a sheltered cove 37 km north east of Bergen, Norway on 12 December 2019. The sphere was suspended about 24 m below the transducers using three monofilament nylon lines approximately on the center of the 70 kHz beam. Ideally, the sphere should be in the center of all four beam, but due to the physical separation of the transducers this is not possible when using practical and achievable sphere ranges. To ensure there was no overlap between the fundamental frequency-bands, the transmitted frequency bands were set to 34-43, 47-88, 92-158, and 162-260 kHz for the 38, 70, 120, and 200 kHz transducers, respectively. The pulse duration was 2.048 ms. The echosounders were calibrated using the same sphere and transmit power as used for the measurements.

To show that the transmit power affects the crosstalk level, different power settings for the echosounders were used (Table 3). Power setting 1 is the same as the recommended setting by Korneliussen et al. (2008). The other power settings were selected to reduce the level of higher harmonic generation, based on the simulation results.

III. RESULTS

A. Simulation results

As an example, using the KZK Texas code, both nonlinear and linear propagation of a broadband signal from 38 kHz transducer at three ranges was simulated (Fig. 1). The signal was a frequency modulated sinusoidal with a linear frequency sweep between ~34 to 45 kHz, duration of 2.048 ms, and an input power of 2000 W to the ES38-7 transducer with assumed 75% electroacoustic efficiency. The non-linearity parameter B/A was set to 5.3, which is appropriate for seawater (Beyer, 1998). The time-domain waveform and its energy flux spectral density (EFSD) level (Carey, 2006) was calculated at 0, 10, and 40 m range from the transducer (Fig. 1) to illustrate the nonlinear wave distortion and harmonic generation. The nonlinearly generated second and third harmonics (red curves) build up in the water and reach a maximum at a distance, then decay. To find where the maximum nonlinearity occurs for this simulation, the amount of nonlinear generation was estimated as the ratio of the energy in the second harmonic band relative to the energy in the fundamental band. The maximum value occurred at around 150 m range.

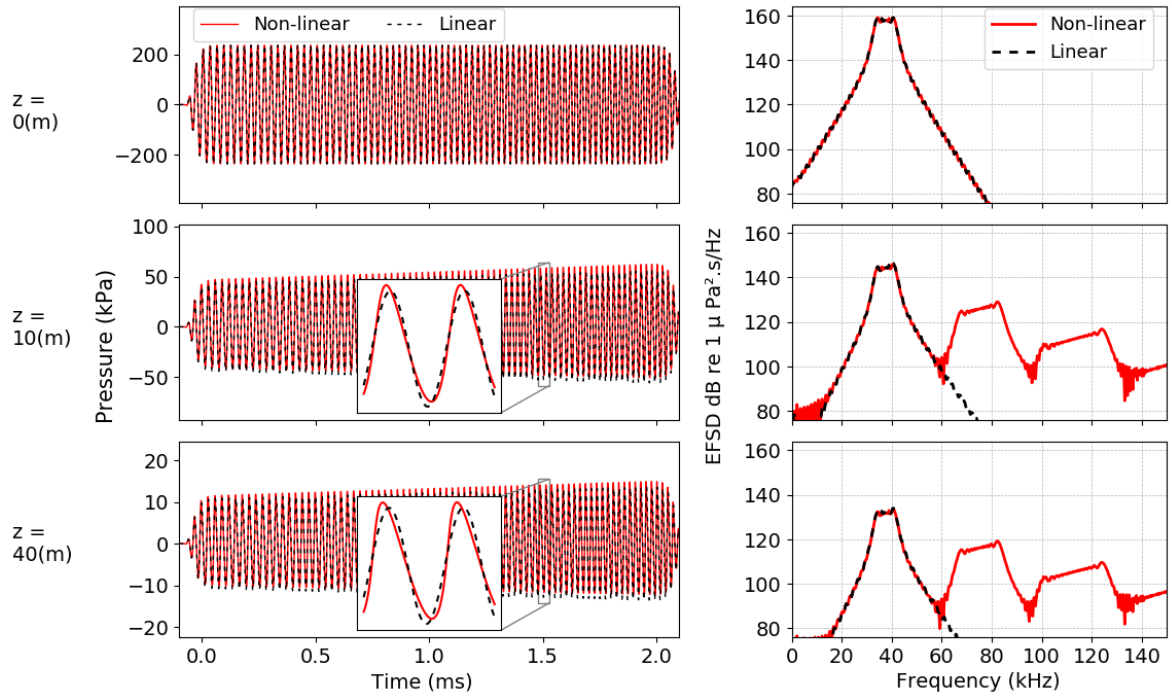

Fig. 1. Modeled generated signal from an unfocused, i.e. flat, acoustic transducer with a uniform pressure on its surface for two cases of nonlinear and linear acoustic propagation. Simulated time waveforms (left panels) at three ranges z=0, 10 and 40 m from the transducer with radius of 160 mm and electroacoustic efficiency of 75% for input power of 2000 W. The pulse had a 2.048 ms duration and a sinusoidal linear frequency sweep between 34-45 kHz with fast tapering or ramping (abrupt raise and fall of the signal (see Demer et al. 2017)) for 2000 W input power. The distortion of the waveform due to the nonlinear propagation is shown in the zoomed windows. The energy spectrum of each time waveform is shown in the right panels.

The KZK Texas code was then used to simulate nonlinear acoustic propagation of the waveform from the four transducers using transmit powers identical to the default power settings of the EK80 echosounder system. The energy spectra at 0, 10, 40, and 200 m from the transducer were calculated to investigate the change in harmonic levels with power (Fig. 2). The maximum amount of nonlinear generation (a ratio of the energy in the second harmonic band compared to the fundamental band) for the 38, 70, 120, and 200 kHz bands at their maximum input powers was estimated to occur at around 150 m, 75 m, 45 m, and 25 m, respectively

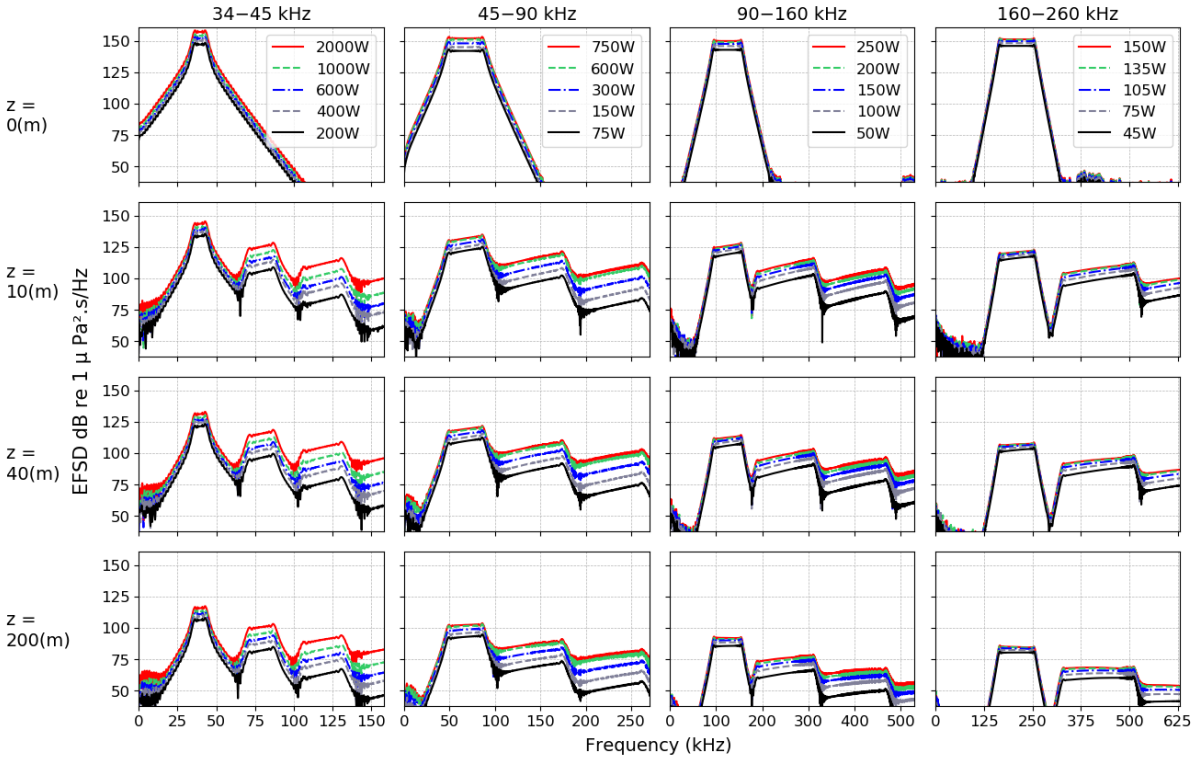

297

298 Fig. 2. Energy flux spectrum density of simulated broadband signals for different input powers in four different
299 transducers (from left to right: 38, 70, 120, and 200 kHz transducers) at four ranges from the transducer surface: 0
300 m, 10 m, 40 m, and 200 m. Each column corresponds to one of the frequency bands and each row to one of the
301 distances.

302 It is clear that by reducing the energy in the fundamental frequency band, comparatively less energy is
303 transmitted to the higher harmonics, as is illustrated by the 10 m range waveforms (Fig. 3). However,
304 the reduction is much larger than the transmit power reduction, suggesting the crosstalk problem may
305 be alleviated by reducing the transmit power for some of the transducers. For example, by reducing the
306 70 kHz transmit power by 4 dB, a reduction of harmonic frequencies of around 8 and 12 dB occurs for
307 the second and third harmonics, respectively. By reducing the output power by around 10 dB, the
308 second and third harmonics are reduced by around 20 and 29 dB, respectively. A similar relationship
309 between reduced transmit power and reduced generation of harmonic frequencies occurs for all
310 frequencies. That is, the relationship between reduction in the EFSD of the harmonics compared to the
311 main band is frequency independent.

312

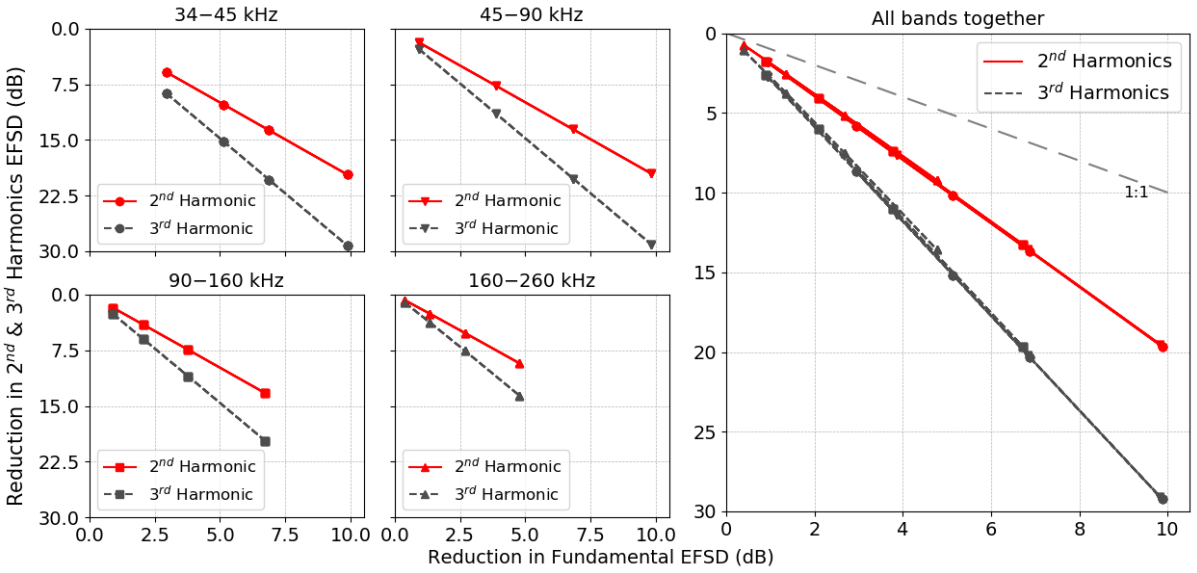

Fig. 3. Reduction in the energy flux spectral density (EFSD) at mid-frequency of the fundamental frequency band and the corresponding reductions in its 2nd and 3rd harmonics at 10 m range from the transducer based on the simulation results. To better visualize the reduction of energy in higher harmonics compared to the reduction of energy in the fundamental frequency band, the 1:1 line is shown by the dashed grey line in the right-hand side panel.

1. *Echosounder power setting to reduce crosstalk based on the numerical modeling*

To minimize the crosstalk interference for the simultaneous operation of broadband echosounders, the results of numerical simulation of nonlinear propagation were used (section B). Reducing the transmit power, the energy in the second and third harmonics drops more than the fundamental frequency band (Fig. 2 and Fig. 3). Therefore, by reducing the transmit power in the lower frequency bands and increasing the power for the highest band, it is possible to reduce the ratio of crosstalk energy to useful energy and hence reduce the cross-channel interference. Simulations at different transmit power settings show that a marked reduction in crosstalk can be achieved and that it varies with range from the transducer. For example, Δ_1 (Fig. 4) shows the difference between the energy of the second harmonic of 38 kHz and the fundamental band of 70 kHz at 82 kHz for power settings 1 and 2 (Table 3). Changing from power setting 1 to power setting 2, Δ_1 is increased from 8 to 18 dB and 4 to 14 dB at 10 m and 40 m, respectively. Similarly, Δ_2 shows the difference between the energy of the second harmonic of 70 kHz and the fundamental energy of 200 kHz at 170 kHz. It increased from -2 (i.e., that

the second harmonic of 70 kHz is stronger than the fundamental at 200 kHz) to 19 dB and -4 to 16 dB at 10 m and 40 m, respectively, by changing from power setting 1 to 2.

Table 3. Different power settings used in the simulations and measurements. The frequency ranges used in the measurements are given in Table *1*. Power setting 1 is per the recommendations in Korneliussen et al. (2008).

Transducer model	ES38-7	ES70-7C	ES120-7C	ES200-7C
Power setting 1 (W)	2000	750	250	105
Power setting 2 (W)	200	75	50	150
Power setting 3 (W)	200	75	50	105
Power setting 4 (W)	400	150	100	135

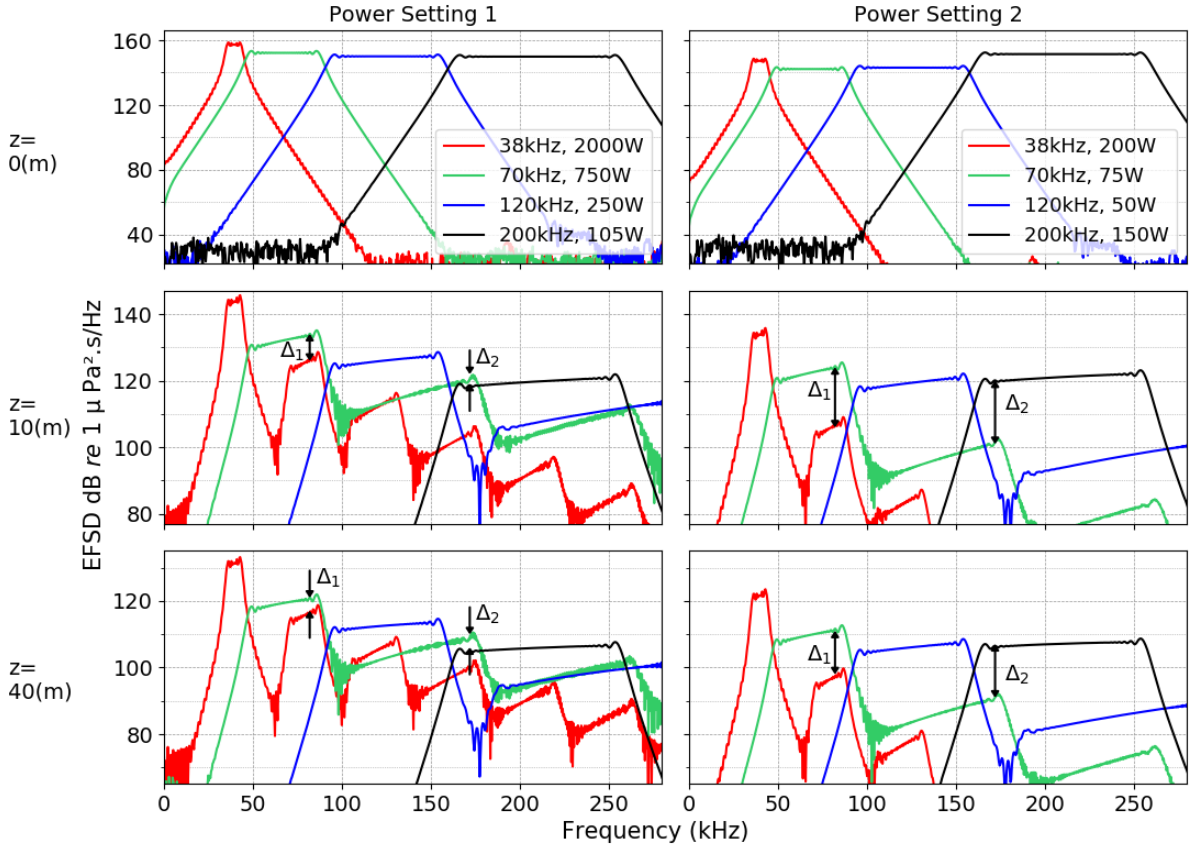

Fig. 4. Simulated energy flux spectral density of broadband signals for two power settings for four frequency bands at 0, 10, and 40 m range. The left panels show the modeled energy using power setting 1 (Table 3). The right

panels present the same output but with power setting 2 (Table 3). The higher harmonic energy is much weaker with the reduced transmit power.

B. Seafloor measurements

The volume backscattering strength of the seafloor was measured as a function of frequency in four bands (Fig. 5) using different configurations (Table 2). The vessel was drifting so the measurements were not taken at exactly the same location. It was observed that backscattering strength in the 38 kHz band is approximately 3, 4, and 3 dB higher compared to the 70, 120 and 200 kHz bands, respectively.

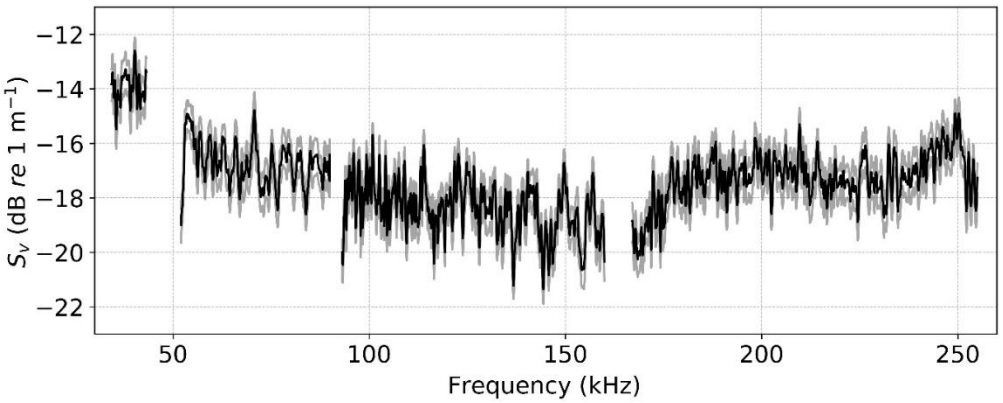

Fig. 5. The mean volume backscattering strength (S_v) from the seafloor (black line) and 95% confidence interval (CI, gray lines). Data from measurements 1, 5, 9 and 10 (Table 2) were used.

1. *Comparison between measurements and modeling results*

To facilitate comparison of the model and measured seafloor backscatter, the EFSD (Fig. 2) and S_v values (as per Eq. (15)) were normalized by transforming both to decibels and setting the maximum value to zero. This was done for both the 38 kHz (using measurements 1-4, Table 2) and 70 kHz transducers (measurements 5-8, Table 2).

For 38 kHz (Fig. 6), since the backscattered energy from seafloor is approximately ~3 to 4 dB higher in the 38 kHz band compared to the other frequencies (see Fig. 5), the measured S_v in the 70 and 120 kHz bands were shifted upward by 3 and 4 dB, respectively. This removes the effects of the seafloor

on the higher harmonics compared to the fundamental band. This measurement confirms that the reduction in higher harmonics with reducing transmit power occurs in a similar manner as the trend from the simulations. For example, the difference between the measured energy in the fundamental band and mid-frequency of the second harmonic band was around 10 dB when the input power was 2000 W and around 20 dB when the input power was 600 W. The other observation is that the measured second and third harmonic energy is higher than predicted from modeling when the input power was 2000 and 1000 W. By reducing the input power to 600 W, the measured energy of the second harmonic was in better agreement with the one predicted by modeling. When decreasing the input power to 200 W the measured harmonic energy becomes less than that predicted from the modeling.

At 70 kHz (Fig. 6), the backscattered energy from the seafloor was ~1 dB higher than in the 120 kHz band and more or less the same level as the 200 kHz band (Fig. 5). Accordingly, to remove the effects of the seafloor between different channels, the measured S_v in the 120 kHz band was shifted upward by 1 dB. In the same way as for 38 kHz, reducing the transmit power will reduce the energy of higher harmonics more than the relative reduction of transmit power. Furthermore, the measured backscattered energy of the second and third harmonic is stronger than those from modeling for the 750 and 600 W input power and by reducing the input power it systematically reduces and ends up below the energy predicted from modeling. In the simulation, the only source of harmonic generation is the nonlinear propagation of acoustic waves. In the measurements, other factors such as instrument characteristics can contribute to the harmonic generation.

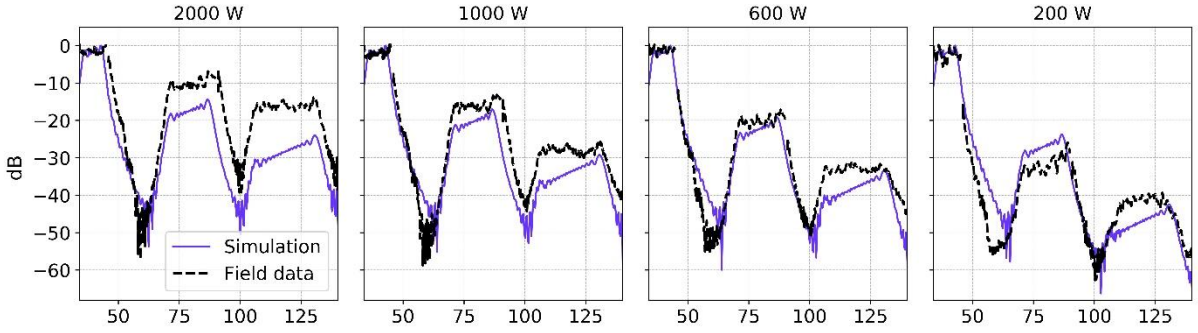

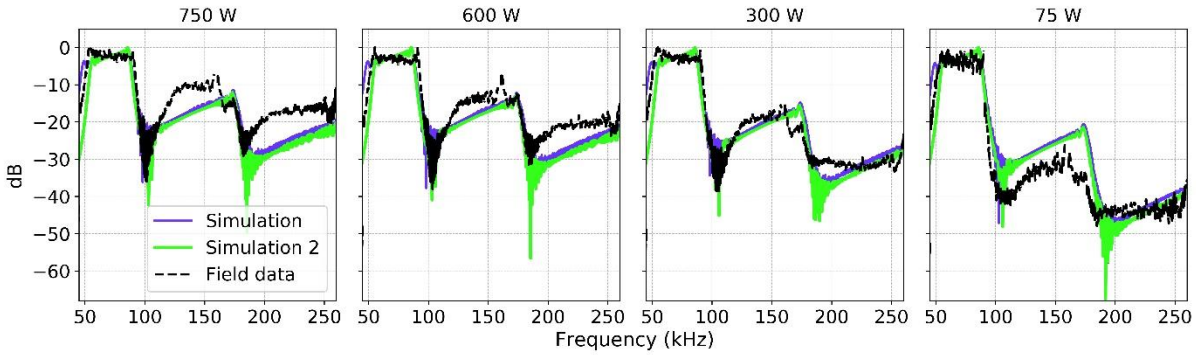

386

387 Fig. 6. Normalized simulated (blue curve) and normalized S_v from seafloor measurements (black curve) for different
388 power settings. Top row: Active transmission by the 38 kHz transducer and passive for the remainder of the
389 channels (measurement configurations 1-4 in Table 2). The passive channels (i.e. 70 and 120 kHz transducers)
390 were used to record the signal in their frequency band. Bottom row: active transmission by the 70 kHz transducer
391 and passive for the remainder (measurement configuration 5-8 in Table 2). The passive channels (i.e. 120 and
392 200 kHz transducers) were used to record the signal in their frequency band. Simulation 1 of the 70 kHz channel
393 has bandwidth 45-90 kHz (Table 1), while Simulation 2 has bandwidth 53-89 kHz with slightly steeper tapering (i.e.
394 shorter rise and fall times) of the signal. In simulation 2, the dip (valley) between the main and second harmonic
395 band is captured for powers 750, 600, and 300 W.

396

397 ## C. Calibration sphere TS measurements with different power settings

398 A calibration sphere suspended about 24 m beneath the transducers was measured (see section II.C.2).
399 The pulse-compressed echograms together with three individual pings for four echosounder channels
400 using power settings 1 and 2 (see Table 3) are shown in Fig. 7 and Fig. 8, respectively. The energy
401 leaking into the higher harmonics of the initial transmitted frequency band can interfere with the
402 neighboring primary bands and generate artifacts appearing above or below the target in the
403 echograms. When echosounders are operating with power setting 1 (Table 3), crosstalk is observed
404 above and below the sphere location (Fig. 7) especially for the 120 and 200 kHz channels (second row
405 panels). With power setting 2 (Table 3), the crosstalk echoes are reduced in the pulse-compressed
406 echograms (Fig. 8).

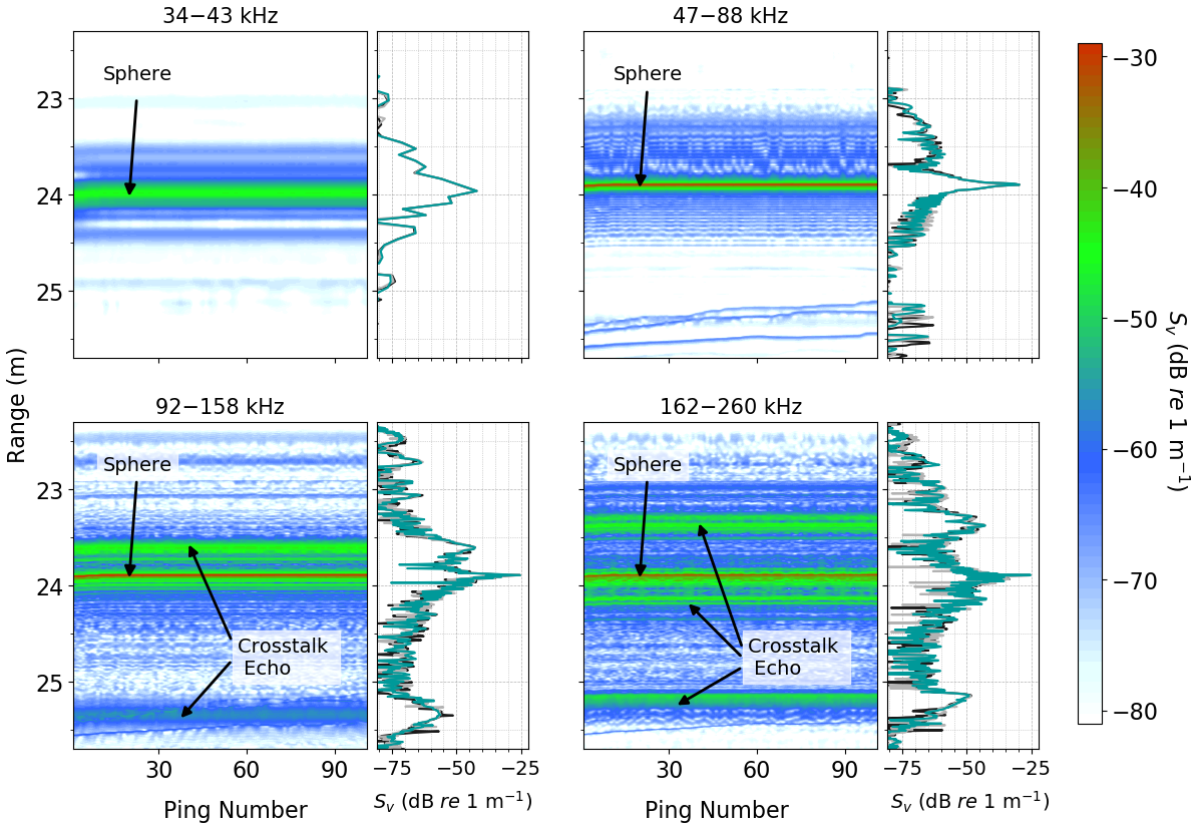

407

408 Fig. 7. Illustration of the crosstalk in pulse-compressed echograms. Four broadband echosounder channels were
409 operated simultaneously using power setting 1 (see *Table 3*). The pulse duration of transmitted signals was 2.048
410 ms. The pulse-compressed echoes from a 38.1 mm diameter tungsten carbide sphere (with 6% cobalt binder) 24
411 m below the transducers are shown for the echosounder channels for 100 successive pings. The S_v for ping
412 numbers 20, 50 and 80 are shown to the right of each echogram. For the 92-158 and 162-260 kHz bands there
413 are strong confounding echoes above and below the sphere due to the crosstalk. -The spacing between the artifacts
414 and the main target is due to the pulse-compression procedure and is explained in the Section III.C.1.

415

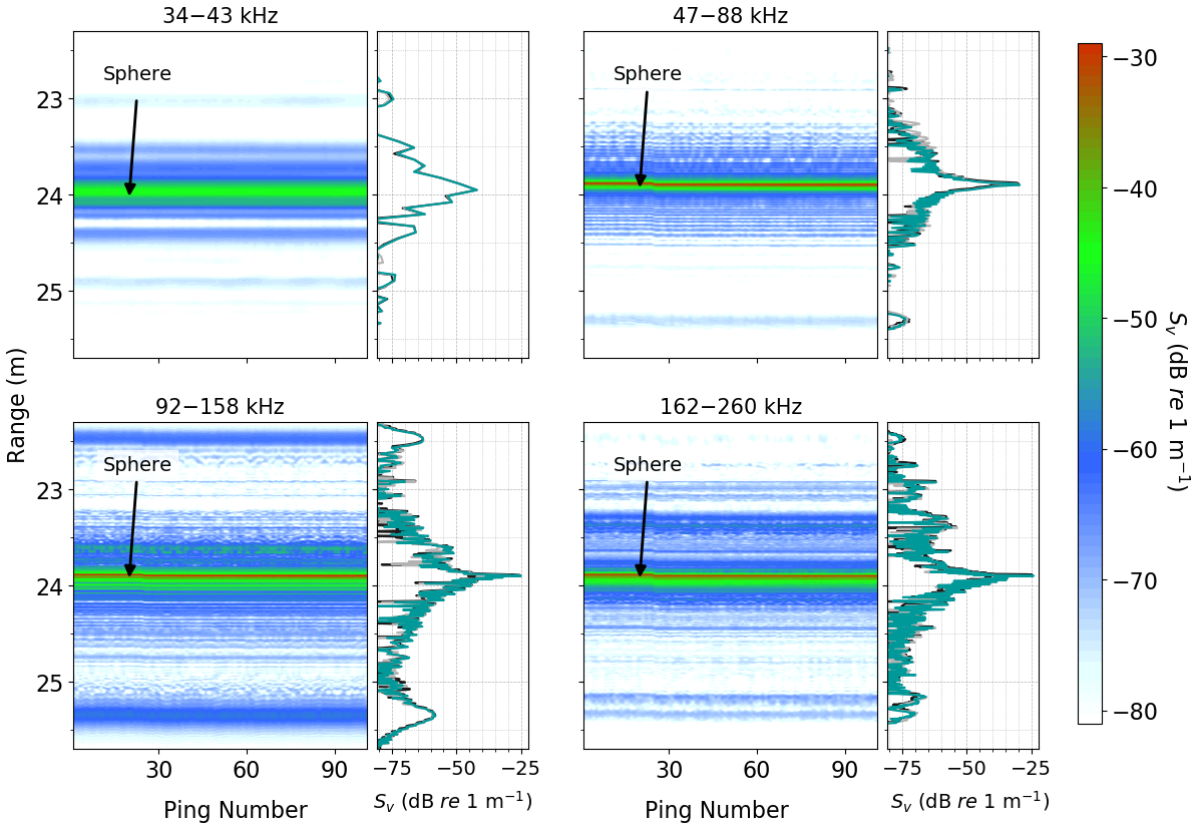

Fig. 8. Demonstration of the reduction of crosstalk with transmit power setting 2. These results were obtained from the same setup as shown in Fig. 7 but with power setting 2. The pulse-compressed echograms are formed by 100 successive pings. The S_v for pings 20, 50 and 80 are shown to the right of each echogram.

To compare the effect of crosstalk on the backscattered energy within the water column around the sphere, the area backscattering coefficient, s_a(m^2 m^{-2}), was calculated between 22-26 m range for power settings 1 and 2 (Fig. 7 and Fig. 8). The percentage change in area backscattering coefficient for power setting 1 (s_{a1}) relative to that of power setting 2 (s_{a2}) and corresponding change in area backscattering strength, S_a ($= 10\log_{10}(s_a)$) was calculated (Table 4). The energy in the 38 and 200 kHz frequency bands was higher for power setting 2. However, the magnitude of the differences is smaller than the estimated calibration variability for these channels (Table 5). On the other hand, the energy in the 70 and 120 kHz frequency bands was higher for power setting 2 and the magnitude is larger than the calibration uncertainty, especially for the 120 kHz frequency band.

Table 4. Change in the area backscattering coefficient, s_a, and area backscattering strength, S_a, between 22-26 m ranges for power setting 1 (Fig. 7) compared to power setting 2 (Fig. 8). Subscript 1

and 2 indicated power settings 1 and 2, respectively. s_a values are estimated by the processing software.

	34-43 kHz	47-88 kHz	92-158 kHz	162-260 kHz
$(s_{a1} - s_{a2})/\, s_{a2}$ (%)	-2.0	2.5	8.9	-0.9
$S_{a1}(\mathrm{dB}) - S_{a2}(\mathrm{dB})$	-0.09	0.11	0.37	-0.04

Table 5. Root mean square (rms) calibration uncertainty (dB) for power settings 1 and 2. Each channel was calibrated separately (i.e., one channel active at a time).

	34-43 kHz	47-88 kHz	92-158 kHz	162-260 kHz
Calibration error (rms)[1] for power setting 1 (dB)	0.14	0.08	0.09	0.15
Calibration error (rms) for power setting 2 (dB)	0.14	0.08	0.1	0.16

1. From SIMRAD EK80 Software.

Furthermore, the distribution of energy within the 22-26 m range for the two power settings was estimated for above (22-23.8 m), around (23.8-24.2 m), and below (24.2-26 m) the sphere at four frequency bands (Table 6). When the crosstalk generation is higher (i.e., 120 and 200 kHz frequency bands in Fig. 7), larger portion of the energy appears above and below the sphere compared to the case of reduced crosstalk (Fig. 8).

Table 6. Distribution of area backscattering coefficient for three depth ranges between 22-26m for power settings 1 and 2 at four different frequency bands.

	34-43 kHz		47-88 kHz		92-158 kHz		162-260 kHz	
	s_{a1}%	s_{a2}%	s_{a1}%	s_{a2}%	s_{a1}%	s_{a2}%	s_{a1}%	s_{a2}%
22 m-23.8 m	1.7	1.7	0.9	0.6	9.5	1.5	9.8	0.8
23.8 m-24.2 m	97	96.6	98.7	99.2	89.3	97.8	85.9	99.0
24.2 m-26 m	1.3	1.7	0.4	0.2	1.2	0.7	4.3	0.2

1. *Pulse-compressed echogram artifacts*

In the echograms for power setting 1 (Fig. 7), crosstalk artifacts appear around 0.3 m above and 1.5 m below the sphere location in the 120 kHz channel and around 0.6 m above, and 0.1 m and 1.2 m below

the sphere in the 200 kHz channel. The offsets between the artifacts and main signal are too large to be explained by the different travel times caused by the spacing between the transducers. Rather, the offsets are mainly due to differences between the frequency band of the matched-filter replica signal and the higher harmonics of other channels. For the sphere measurements (Fig. 7), the fundamental signal of the 70 kHz channel covers the frequency band of 47—88 kHz within 2.048 ms. Its associated second harmonic covers 94—166 kHz within the same time period. The matched filter for a 120 kHz channel with the same period covers the 92-158 kHz band and will produce the best match earlier in the pulse than would be expected. This causes the second harmonic to appear at a closer range on the 120 kHz channel than the first harmonic does on the base channel.

To further clarify the observed offsets in the echogram, as an example, consider an echosounder system with four channels 38, 70, 120, and 200 kHz. They transmit 2.048 ms broadband pulses with 34—43, 47—88, 92—158, and 162—260 kHz frequency bands, respectively. All of them had unit amplitude with a linear frequency sweep at a sampling frequency of 4.096 MHz. For simplicity, the replica signals for the pulse compression of the higher harmonic signals also had unit amplitude. Furthermore, to exclude the travel time offset, we have assumed that there is no travel time difference between receiver channel own signal and the signal of another channel. As shown in Fig. 9, the 120 kHz channel receives its own signal (Line A), second harmonic of 70 kHz (Line B), and third harmonic of 38 kHz (Line C). The signals were convolved with a signal of 120 kHz and normalized by the matched filter magnitude of the 120 kHz channel convolved with itself (Fig. 9). Prior to convolution, all the signals were passed through a bandpass filter with lower and higher bounds (92 and 158 kHz, respectively) as used by the 120 kHz channel. No decimation was applied to the signals. The 200 kHz channel receives its own signal (Line D: 162—260 kHz), the second harmonic of 120 kHz (Line E), second and third harmonics of 70 kHz (Line F and Line G, respectively). These signals were convolved with a 200 kHz replica signal and normalized by the matched filter magnitude of the 200 kHz channel convolved with itself (Fig. 9). As for the previous example, prior to convolution all the signals were passed through a bandpass filter with lower and higher bounds (162 and 260 kHz, respectively) as used by the 200 kHz channel. No decimation was applied to the signals. The convolution of second harmonic of 70 kHz and the fundamental signal of 200 kHz is very weak compared to the others.

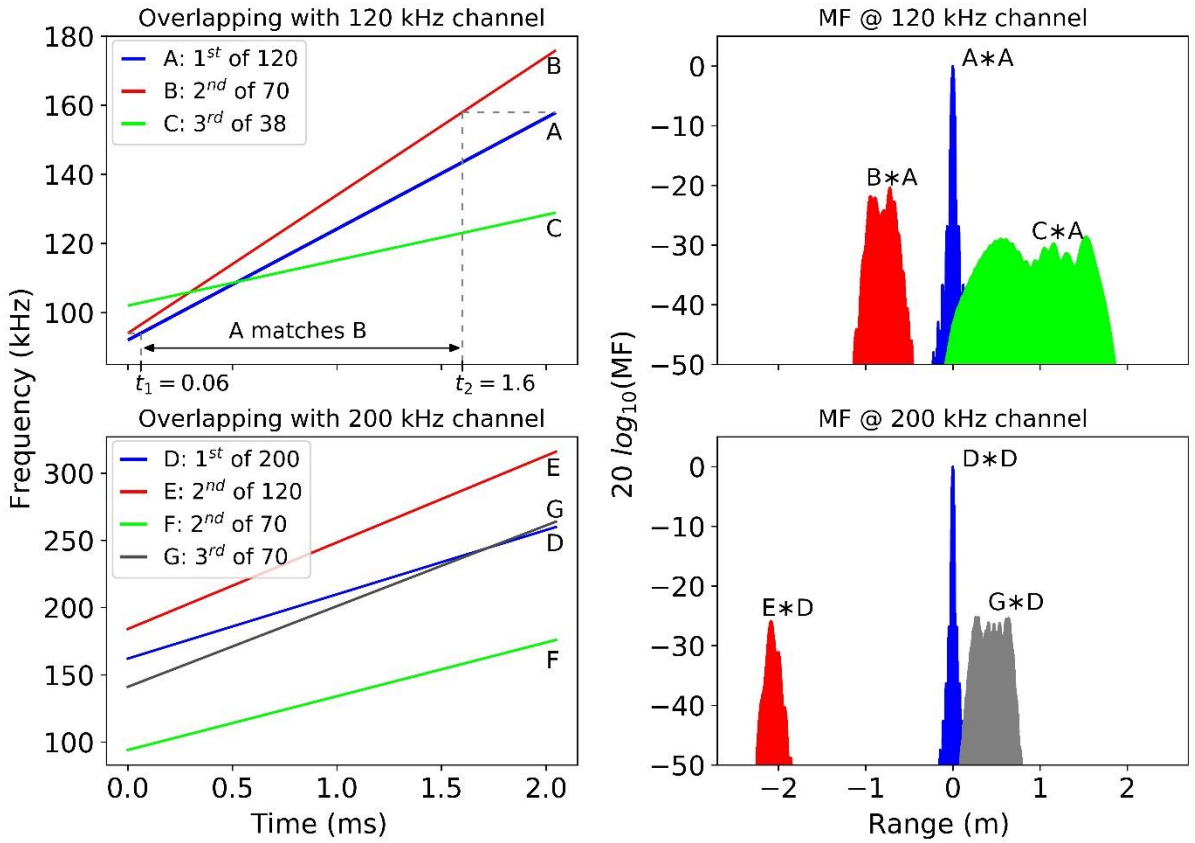

Fig. 9. Pulse compression (or matched filtering) for overlapping signals of 38, 70, 120 and 200 kHz channels is illustrated by an example. They transmit 2.048 ms broadband pulses with 34—43, 47—88, 92—158, and 162—260 kHz frequency bands, respectively. Top left: signals received by the 120 kHz channel are the signal by itself (Line A: 92—158 kHz), second harmonic of 70 kHz (Line B: 92—166 kHz) and third harmonic of 38 kHz (Line C: 102—129 kHz). Where A produces the best match with B is shown. Top right: matched filter of "A", "B", and "C" with "A" are plotted after normalization by matched filter of A with itself. Bottom left: signals received by the 200 kHz channel are the fundamental signal by 200 kHz (Line D: 162—260 kHz), second harmonic of 120 kHz (Line E: 184—316 kHz), second and third harmonics of 70 kHz (Line F: 92—166 and Line G: 141—264 kHz, respectively). Bottom right: matched filter of "D", "E", "F", and "G" with "D" are plotted after normalization by matched filter of D with itself. X-axis of the right panels is converted to range by multiplying the time signal by the sound speed of water (1500 m/s).

2. *TS estimation for different power settings using different window length*

493 The measured backscattered target strength can be distorted by crosstalk. For the experiment
494 conducted in this paper, this deviation in TS measurements of five successive pings was up to 10-15
495 dB in the higher frequencies (e.g., Fig. 10). The TS for each ping was estimated from a Fourier transform
496 of the pulse-compressed signal in the processing software. The crosstalk distortion effects on the
497 estimated TS from pulse-compressed signals varies depending on different power settings and different
498 Fourier transform window lengths (see Fig. 10).

499 One way to reduce the effect of crosstalk on TS estimation in the processing stage is to select Fourier
500 transform window lengths around the main target that avoid including the artifacts (Fig. 10). The target
501 location can be selected from the pulse-compressed echograms of the lower frequency bands where
502 artifacts are not present. However, some of the artifacts might be too close to the main signal and can
503 therefore not be excluded by a shorter window length. The penalty of selecting a shorter window length
504 is a reduced frequency resolution. A window shorter than a certain length removes part of the target's
505 signal. An alternative is to reduce the transmit power of the lower frequency transducer channels to
506 reduce the energy transmitted into the higher harmonics. In this case the measured target strength
507 closely match the theoretical TS, independent of the Fourier window length (Fig. 10). The cost of
508 decreasing the transmit power is reduced SNR in the main band, which can be clearly observed (Fig.
509 2).

510

511

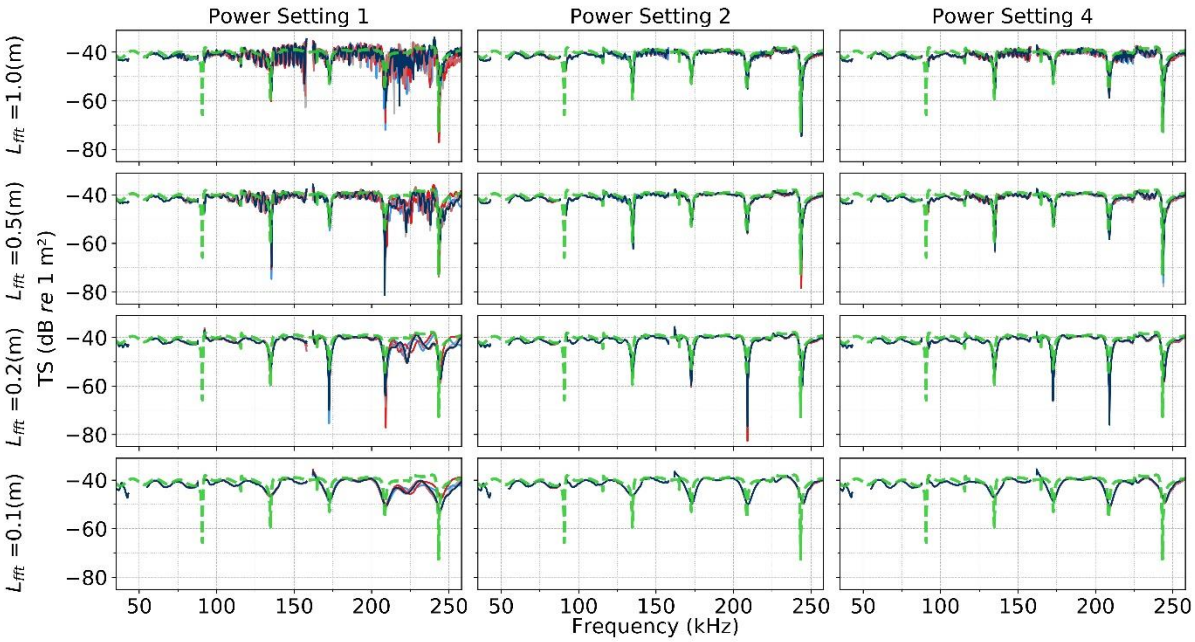

512

513 Fig. 10. Solid lines (—): measured TS for a ping. Dashed line (- - -) Theoretical TS. The measured frequency
514 response of the target strength of a 38.1 mm tungsten carbide sphere for five pings (12 to 16). Varying Fourier
515 window lengths, L_{fft} , of 1, 0.5, 0.2, and 0.1 m for power settings 1 ,2, and 4 (Table 3) demonstrate the effect on
516 target frequency response. The results of the power setting 3 were similar to the power setting 2 and are
517 not shown. The theoretical TS is shown by the dashed green line. For power setting 1 there is a marked deviation
518 of the measured from theoretical above about 120 kHz, especially for longer window lengths.

519

520 Operating the system with power setting 1, crosstalk causes up to 15 dB bias in TS estimation across
521 200 kHz band using a Fourier window length of 1 m. Using the shortest Fourier window length before
522 losing important features such as nulls in the frequency response, the deviation is up to ~5-7 dB above
523 210 kHz. Too short a window length excludes part of the backscattered signal such as Rayleigh surface
524 waves and fails to resolve the null structure. In fact, the minimum required window length depends on
525 the target, its size, and orientation. The null structure is an important feature of the target and can be
526 used for identification purposes. The nulls caused by crosstalk are confounding artifacts and can be
527 difficult to distinguish from target nulls. Therefore, in some circumstances using filtering or smoothing
528 methods to eliminate (or reduce) crosstalk induced nulls would not be a good practice.

529 If this level of bias is unacceptable, using power setting 2 would likely reduce the amount of crosstalk
530 to below 1 dB. The costs, however, are a reduction in SNR of around 10 dB for the 38 and 70 kHz

channels and 5 dB for the 120 kHz channel. Therefore, the operable range is decreased by around 50% for 38 and 70 kHz band and around 25% for 120 kHz band.

IV. DISCUSSION AND CONCLUSIONS

We have investigated harmonic generation due to nonlinear acoustic propagation via the KZK (Khokholov-Zabolotskaya-Kuztetsov) equation, solved by the KZK Texas code. The relative amount of energy transmitted to the higher frequencies as estimated by modeling was validated via a field experiment that measured seafloor backscattering (Fig. 6). For a more quantitative study of crosstalk effects, backscattering from a target sphere of known reflectivity was measured. In the numerical modeling, the generated harmonics are solely due to the nonlinear propagation. Hence for the echosounders we studied, the agreement between the modeled and measured harmonics indicates that a significant portion of observed harmonics arises from nonlinear acoustic propagation through the medium. Knowing the source of the higher harmonics and the magnitude of the distortion caused by the crosstalk interference helps to decide appropriate acoustic data acquisition strategies using echosounders. Using these results, we tested a procedure that provides a notable reduction in the generated higher harmonics and hence crosstalk magnitude (Fig. 8 and Fig. 10) when operating the broadband channels simultaneously. We have also shown possibilities for removing portions of the crosstalk effects in the processing stage.

Backscatter from the seafloor at a depth of around 40 m in a field experiment was recorded over a broad frequency range to investigate nonlinear generation of sound from the echosounders commonly used in fisheries acoustics. For the 38 kHz transducer, reducing the power from 2000 W to 1000 W and then to 600 W, the correspondence between the field and modeling results improved (Fig. 6). This may indicate that part of the waveform distortion in the high input power is due to nonlinearity in the instrument rather than nonlinear effects in the water column during sound propagation. Reducing the power further to 200 W, the predicted 2^{nd} harmonic energy by the model is stronger than for the field measurements. One possible explanation can be that the calibration of the echosounders was performed using a 2000 W power setting. A similar result was obtained for the 70 kHz transducer, despite the agreement between modeling and measurements not being as good as for the 38 kHz transducer. Reducing the power from 750 W to 600 W and to 300 W on the 70 kHz transducer (Fig. 6),

560 the agreement between the measured and modeled results improved. For 75 W input power the
561 predicted 2nd harmonic is stronger than from the measurements, which may be due to the calibration
562 being carried out at the full 750 W transmit power. Reducing the modeled transmit signal bandwidth
563 from 47-90 kHz to 53-89 kHz improves the match to the measurements especially for the dip between
564 the main and second harmonic band. Both modeling results and measurements agree in the sense that
565 reducing the transmission power substantially decreases the relative harmonic energy.

566 From the material presented, we found that a simple way to reduce the level of generated harmonics
567 while simultaneously pinging without significant levels of crosstalk was to reduce the transmit power on
568 the channels which generate the interfering higher harmonics (Table 3, Fig. 4). Backscattering from a
569 metallic sphere was obtained at–different transmit powers (Table 3). For power setting 1, the TS
570 measurements deviate from the predicted target strength (Fig. 10) and there are spurious targets
571 generated (Fig. 7), especially for the 120 and 200 kHz channels. In comparison, power setting 2 resulted
572 in markedly reduced echogram artifacts (Fig. 8) and there was also good agreement between the
573 measured and theoretical TS (Fig. 10). For power setting 2, the transmit power of the lower frequency
574 bands were reduced to reduce the energy in the higher bands (see Fig. 3) but the power of the highest
575 active frequency band was increased from 105 to 150 W. However, based on the simulation results
576 (Fig. 2), it could remain at 105 W without significant reduction in Δ_2 which is demonstrated by power
577 setting 3. It was observed (Fig. 10) that measured TS follows the theoretical with only minor levels of
578 crosstalk. Note that Δ at each frequency is range dependent (Fig. 4). This is because nonlinearly
579 generated sound builds up during propagation at a rate dependent on the strength of the fundamental
580 frequency band, but geometrical spreading and absorption dissipates the energy of the fundamental
581 wave as it propagates, leading to lower peak pressures and hence lower transfer of energy into
582 harmonics.

583 Simultaneous pinging with several broadband systems is a natural extension of multifrequency
584 narrowband systems. Reducing the transmit power decreases the energy in the fundamental band and
585 has results in reduced SNR, which can limit the useful operating range of the echosounders. Depending
586 on the application and operational requirements, another choice of transmit powers might provide a
587 better trade-off between SNR and low harmonic energy generation (e.g., power setting 4 in Table 3,
588 and Fig. 10). In some cases, high SNR is a strong requirement and power reduction below that required
589 to reduce the level of generated harmonics is not feasible. For example, based on the simulation results

(Fig. 4), reducing the transmit power of 120 kHz to 100 or 150 W instead of 50 W might be an acceptable trade-off between TS and SNR enhancement. As an alternative strategy, it may be possible to reduce the crosstalk problem in the processing stage by selection of Fourier transform window lengths when estimating TS from pulse-compressed signals (Fig. 10**Error! Reference source not found.**). However, depending on the spacing between the crosstalk effects and the main signal, shortening the Fourier window below a certain length decreases the frequency resolution and may not capture relevant features of the scattered signal, depending on its size and orientation. Reduction of crosstalk effects in the processing stage might not be an appropriate strategy if the artifacts are closely located around the main target or if there is an overlap between pulse-compressed harmonics of one target with the main band signal of a neighboring target.

The choice between simultaneous operation of multiple channels with shorter operating range, or longer operating range and sequential operation of channels is an operational decision that should be based on the data needs and constraints. Our results indicate that the crosstalk consequences for volume backscattering and echo-integration are smaller than for target strength measurement.

Fisheries surveys which are conducted in areas where the maximum water depth is less than 200 m do not need high transmit powers at the lower frequencies (e.g., 18, 38 and 70 kHz) and the echosounders can be operated simultaneously with reduced output power with minimal deleterious effects. When changing from power setting 1 to 2, for example, SNR decreases by around 10 dB for 38 and 70 kHz channels and 5 dB for the 120 kHz channel. Grouped pinging or alternate narrowband and broadband operation may also be utilized if appropriate. Other examples where reduced transmit powers may be directly applicable are for lowered acoustic probes or moored systems where the maximum desired operational range can be less than 100 m and the frequency response from single targets over a wide frequency range is valuable.

In this paper, different channels were calibrated separately. Calibration of channels when operating simultaneously would likely account for the cross-talk to some extent, but only at the range of the calibration sphere due to the range-dependence of the cross-talk (e.g. Fig. 2).

ACKNOWLEDGEMENTS

This research was funded by the Institute of Marine Research, Norway. The research project HARMES (Harvesting the Mesopelagics — Ecological and Management Implications), MEESO, and Research Council of Norway (project number 280546) and the EU H2020 research and innovation programme (Grant Agreement No 817669) and the Center for Research-based Innovation in Marine Acoustic Abundance Estimation and Backscatter Classification (CRIMAC) (Project No. 309512) (www.crimac.no) are acknowledged for financial support. We are grateful to M.F. Hamilton and R.O. Cleveland for responding to our questions regarding the Texas code. L.N. Andersen is acknowledged for the fruitful discussions related to nonlinear harmonic generation and his suggestions that improved the structure of the paper. R. Kubilius is thanked for helping with the data collection of the first experiment. Two anonymous reviewers are acknowledged for providing detailed comments and invaluable suggestions that markedly improved the quality of the manuscript.

REFERENCES

Andersen, L.N., Ona, E. and Macaulay, G. (**2013**). Measuring fish and zooplankton with a broadband split beam echo sounder. In 2013 MTS/IEEE OCEANS-Bergen (pp. 1-4). IEEE.

Averkiou, M.A. and Hamilton, M.F. (**1997**). Nonlinear distortion of short pulses radiated by plane and focused circular pistons. J. Acoust. Soc. Am. **102**(5), pp. 2539-2548.

Bassett, C., De Robertis, A., and Wilson, C.D. (**2018**). Broadband echosounder measurements of the frequency response of fishes and euphausiids in the Gulf of Alaska. ICES J. Mar. Sci. **75**(3), pp. 1131-1142.

Beyer, R.T. (**1998**) "The Parameter B/A," in *Nonlinear Acoustics*, edited by M.F. Hamilton and D.T. Blackstock, Chap. 2, pp. 25–40 (Academic Press, San Diego).

Blanluet, A., Doray, M., Berger, L., Romagnan, J.B., Le Bouffant, N., Lehuta, S. and Petitgas, P. (2019). Characterization of sound scattering layers in the Bay of Biscay using broadband acoustics, nets and video. PloS one, **14**(10).

Carey, W.M., (**2006**). Sound sources and levels in the ocean. EEE J. Oceanic Eng., **31**(1), pp.61-75.

Chu, D. and Stanton, T.K. (**1998**). Application of pulse compression techniques to broadband acoustic scattering by live individual zooplankton. J. Acoust. Soc. Am. **104**(1), pp. 39-55.

646 Chu, D. (**2011**). Technology evolution and advances in fisheries acoustics. J. Mar. Sci. Technol., **19**(3), pp. 245-
647 252.

648 Cleveland, R.O., Hamilton, M.F. and Blackstock, D.T. (**1996**). Time-domain modeling of finite-amplitude sound in
649 relaxing fluids. J. Acoust. Soc. Am. **99**(6), pp. 3312-3318.

650 Demer, D.A., Andersen, L.N., Bassett, C., Berger, L., Chu, D., Condiotty, J., Cutter, G.R., Hutton, B., Korneliussen,
651 R., Bouffant, N.L., Macaulay, G., Michaels W.L., Murfin, D., Pobitzer, A., Renfree, J.S., Sessions, T.S., Stierhoff,
652 K.L., and Thompson C.H. (**2017**). USA — Norway EK80 Workshop Report: Evaluation of a wideband echosounder
653 for fisheries and marine ecosystem science. *ICES Cooperative Research Report*, *336*, p. 69

654 Duck, F.A., (**2002**). Nonlinear acoustics in diagnostic ultrasound. Ultrasound Med. Biol., **28**(1), pp.1-18.

655 Foote, K.G. and MacLennan, D.N. (**1984**). Comparison of copper and tungsten carbide calibration spheres. J.
656 Acoust. Soc. Am. **75**(2), pp. 612-616.

657 Francois, R.E. and Garrison, G.R. (**1982**). Sound absorption based on ocean measurements. Part II: Boric acid
658 contribution and equation for total absorption. J. Acoust. Soc. Am. **72**(6), pp. 1879-1890.

659 Greenlaw, C.F. (**1979**). Acoustical estimation of zooplankton populations 1. Limnol. Oceanogr., **24**(2), pp. 226-242.

660 Hamilton, M.F. and Blackstock, D.T. (**1998**). *Nonlinear acoustics* (Vol. 237). (San Diego: Academic press).

661 Hamilton M.F. and Morfey C. L. (**1998**) "Model equations," in *Nonlinear Acoustics*, edited by M.F. Hamilton and
662 D.T. Blackstock, Chap. 3, pp. 41—64 (Academic Press, San Diego).

663 Handegard, N.O., (**2007**). Observing individual fish behavior in fish aggregations: tracking in dense fish
664 aggregations using a split-beam echosounder. J. Acoust. Soc. Am. **122**(1), pp.177-187.

665 Holliday, D.V., Pieper, R.E. and Kleppel, G.S. (**1989**). Determination of zooplankton size and distribution with
666 multifrequency acoustic technology. ICES J. Mar. Sci. **46**(1), pp. 52-61.

667 Horne, J. (**2000**). Acoustic approaches to remote species identification: a review. Fish. Oceanogr. **9**(4): 356-371.
668 Jech, J.M., Lawson, G.L. and Lavery, A.C. (**2017**). Wideband (15–260 kHz) acoustic volume backscattering spectra
669 of Northern krill (Meganyctiphanes norvegica) and butterfish (Peprilus triacanthus). ICES J. Mar. Sci. **74**(8), pp.
670 2249-2261.

671 Jones, E., Oliphant, T. and Peterson, P., (**2001**). SciPy: Open source scientific tools for Python. URL http:
672 //www.scipy.org/.

673 Korneliussen, R.J. and Ona, E. (**2002**). An operational system for processing and visualizing multi-frequency
674 acoustic data. ICES J. Mar. Sci. **59**(2), pp. 293-313.

675 Korneliussen, R., Ona, E., Eliassen, I., Heggelund, Y., Patel, R., Godø, O., Giertsen, C., Patel, D., Nornes, E., and
676 Bekkvik, T. (**2006**). "The large scale survey system-LSSS," in Proceedings of the 29th Scandinavian Symposium
677 on Physical Acoustics, Ustaoset.

678 Korneliussen, R.J., Diner, N., Ona, E., Berger, L. and Fernandes, P.G. (**2008**). Proposals for the collection of
679 multifrequency acoustic data. ICES J. Mar. Sci. **65**(6), pp. 982-994.

680 Korneliussen, R.J. (**2010**). The acoustic identification of Atlantic mackerel. ICES J. Mar. Sci. **67**(8), pp. 1749-1758.

681 Korneliussen, R., Heggelund, Y., Macaulay, G. J., Patel, D., Johnsen, E., and Eliassen, I. (**2016**). Acoustic
682 identification of marine species using a feature library. Methods in Oceanogr., 17 pp. 187—205.
683 https://doi.org/10.1016/j.mio.2016.09.002

684 Kuo, S.M., Wu, H.T., Chen, F.K. and Gunnala, M.R., (**2004**). Saturation effects in active noise control
685 systems. IEEE Trans. Circuits Syst. I Regul. Pap., **51**(6), pp.1163-1171.

686 Lawrence, E.K., Austin, R.F., Alan, B.C. and James, V.S. (**2000**). *Fundamentals of acoustics*. (New York: John
687 wileys)

688 Lee, Y.-S. (**1993**). ‘‘Numerical solution of the KZK equation for pulsed finite amplitude sound beams in
689 thermoviscous fluids,’’ Ph.D. dissertation, The University of Texas at Austin, Austin, TX.

690 Lee, Y.S. and Hamilton, M.F. (**1995**). Time-domain modeling of pulsed finite-amplitude sound beams. J. Acoust.
691 Soc. Am. **97**(2), pp. 906-917.

692 Liu, S., Croxford, A.J., Neild, S.A. and Zhou, Z., (**2011**). Effects of experimental variables on the nonlinear harmonic
693 generation technique. IEEE Trans. Ultrason. Ferroelectr. Freq. Control, **58**(7), pp.1442-1451.

694 MacLennan, D.N., (**1981**). The Theory of Solid Spheres as Sonar Calibratiom Targets. *Scott. Fish. Res. Rep*.

695 Matlack, K.H., Kim, J.Y., Jacobs, L.J. and Qu, J., (**2015**). Review of second harmonic generation measurement
696 techniques for material state determination in metals. J. Nondestr. Eval., **34**(1), p.273.

697 Novikov, B.K., Rudenko, O.V. and Timoshenko, V.I. (**1987**). *Nonlinear underwater acoustics* (p. 36). (New York:
698 American Institute of Physics.)

699 Ona, E., ed. (**1999**). “Methodology for Target Strength Measurements,” ICES Cooperative Research Report
700 International Council for the Exploration of the Sea, Vol. **235**.

701 Pedersen, A. (**2006**). “Effects of nonlinear sound propagation in fisheries research”. PhD dissertation, University of
702 Bergen, Norway. 308 pp.

Pierce, A.D., (**1989**). *Acoustics: an introduction to its physical principles and applications*. (Acoustical Society of America, Huntington Quadrangle Melville, NY).

Price, R. (**1956**). Optimum detection of random signals in noise, with application to scatter-multipath communication — I. IEEE Trans. Inf. Theory, **2**(4), pp. 125-135.

Proakis J.G., Manolakis, D.G. (**1996**). *Digital Signal Processing: Principles, Algorithms and Applications* (third edition *Pentice-Hall*, New Jersey)

Rossing, T. D. (**2007**). *Springer Handbook of Acoustics*. Springer, New York.

Stanton, T.K., Chu, D., Jech, J.M. and Irish, J.D. (**2010**). New broadband methods for resonance classification and high-resolution imagery of fish with swimbladders using a modified commercial broadband echosounder. ICES J. Mar. Sci. **67**(2), pp. 365-378.

Stanton, T.K., Reeder, D.B. and Jech, J.M. (**2003**). Inferring fish orientation from broadband-acoustic echoes. ICES J. Mar. Sci. **60**(3), pp. 524-531.

Simmonds, E.J. and MacLennan, D.N. (**2005**). *Fisheries acoustics theory and practice*. Blackwell Publishing.

Sund, O. (**1935**). Echo sounding in fishery research. Nature, **135** (3423), p.953.

Tichy, F.E., Solli, H. and Klaveness, H. (**2003**). Nonlinear effects in a 200-kHz sound beam and the consequences for target-strength measurement. ICES J. Mar. Sci. **60**(3), pp. 571-574.

Trenkel, V.M., Ressler, P.H., Jech, M., Giannoulaki, M. and Taylor, C. (**2011**). Underwater acoustics for ecosystem-based management: state of the science and proposals for ecosystem indicators. Mar. Ecol. Prog. Ser. 442, pp. 285-301.